Influence of large-scale climate signals on theprecipitation variability over Iran

Zohreh Javanshiri (javanshirizohreh@gmail.com)
Climate Research Institute (CRI), Atmospheric Science and Meteorological Research Center (ASMERC)
Iman Babaeian
Climate Research Institute (CRI), Atmospheric Science and Meteorological Research Center (ASMERC)
Morteza Pakdaman
Climate Research Institute (CRI), Atmospheric Science and Meteorological Research Center (ASMERC)

Research Article

Keywords: atmosphere-ocean circulation, climate teleconnections, Iran precipitation, wavelet coherence, Persian Gulf

Posted Date: August 25th, 2022

DOI: https://doi.org/10.21203/rs.3.rs-1982295/v1

Influence of large-scale climate signals on the precipitation variability over Iran

Zohreh Javanshiri[1*], Iman Babaeian[1] and Morteza Pakdaman[1]

[1*]Climate Research Institute (CRI), Atmospheric Science and Meteorological Research Center (ASMERC), Mashhad, Iran.

*Corresponding author(s). E-mail(s): javanshirizohreh@gmail.com;
Contributing authors: ibabaeian@yahoo.com; pakdaman.m@gmail.com;

Abstract

This study investigates relationships between the twenty large-scale climate signals and the precipitation variability during 1960–2018 in Iran. The twenty large-scale climate indicators include atmosphere-ocean teleconnections as well as El Niño and Southern Oscillation (ENSO) signals, Pacific and Atlantic ocean Sea Surface Temperature (SST). Wavelet Coherence Analysis (WCA) was applied to detect the impact of climate signals on Iran's monthly precipitation. The results revealed that (a) the significant wavelet coherence and the phase difference between monthly precipitation and climate signals were highly variable in time and periodicity, (b) at inter-annual scale, Iran's precipitation had been linked more to Extreme Eastern Tropical Pacific SST(0°-10°S, 90°-80°W) (Niño 1.2), Oceanic Niño Index (ONI), and Western Hemisphere Warm Pool (WHWP), respectively, (c) decadal and inter-decadal precipitation variability are mainly associated with variability in Atlantic Meridional Mode (AMM), Western Pacific Index (WP) and Arctic Oscillation (AO), and (d) in the most recent decade, the coherence between precipitation and large-scale climate signals has been declined in decade and inter-decade scales, and an unstable coherence has been emerged in annual scale.

Keywords: atmosphere-ocean circulation; climate teleconnections; Iran precipitation; wavelet coherence; Persian Gulf

1 Introduction

The spatio-temporal variability of precipitation is an essential hydro-climatic variable for the planning and management of regional water resources (Jiang et al. (2014)). Also, It has been shown that climatic patterns of large-scale atmospheric circulation significantly affect the variabilities of precipitation (Rathinasamy et al. (2019)). Therefore, the analysis of the relationship between precipitation variability and large-scale climate fluctuations has increased the ability to improve the accuracy of precipitation forecasting, which will be useful for efficient management of water resources.

Many studies have been pursued to investigate the relationship between regional hydrometeorological variables and large-scale climate indicators by various approaches. For example, in Europe, Jevrejeva et al. (2005) used wavelet transform method for studying the influence of large-scale atmospheric circulation of North Atlantic Oscillation (NAO) and AO on sea level rise off the European coast. They detected four dominant signals with periods 2.2, 3.5, 5.2 and 7.8 years by the wavelet transform using time series of sea level typically 150 years long together with the NAO/AO signals.

In Africa, Jemai et al. (2017) studied the variability of precipitation in the southeast of Tunisia through the analysis of data about annual and monthly precipitation at five stations in the watershed of Gabes, from 1977 to 2015. The analysis of wavelet coherence showed a strong correlation between Gabes watershed precipitation and Mediterranean Oscillation (MO) at different temporal scales. Ouachani et al. (2013) assessed the potential impact of large-scale climate patterns of ENSO, NAO and PDO in modulating precipitation regimes across the upper Medjerda River Basin in northern Tunisia. They used wavelet spectra and showed that the ENSO signals are well correlated with precipitations at a time delay of 2 years. Specifically, Niño3.4, Central Tropical Pacific SST(5°N-5°S, 160°E-150°W) (Niño4) and Multivariate ENSO Index (MEI) presented the strongest coefficient of correlation.

For North America, Chang et al. (2017) investigated the systematic relationships between global SST anomalies and terrestrial precipitation variability with respect to long-term nonlinear and non-stationary teleconnection signals during 1981–2010 over three regions in North America and one in Central America. They used machine learning techniques and showed that some unknown teleconnection patterns (e.g., South Pacific pattern in the Central America and the southwestern US sites in winter) had a much higher contribution to precipitation variability when compared to the known teleconnection patterns. Machine learning techniques have widespread applications in climate prediction (for example see Pakdaman et al. (2020), Pakdaman et al. (2022) and Pakdaman et al. (2020)). Jiang et al. (2014) studied the spatiotemporal variability of Alberta's seasonal precipitation, their teleconnection with large-scale climate anomalies and sea surface temperature by using wavelet analysis, Wavelet-based Principal Component Analysis (WPCA), composite analysis and Scale-Averaged Wavelet Power (SAWP) of seasonal precipitation. They showed that warm phases of climate anomalies tend to give rise to dry climate

in Alberta and vice versa. Tan et al. (2016) used variants of wavelet analysis to detect significant interannual and interdecadal oscillations and their teleconnections to large-scale climate anomalies such as ENSO, PDO, and NAO, monthly and seasonal maximum daily precipitation from 131 stations across Canada. They showed that both ENSO and PDO modulated the interannual variability and PDO modulated the interdecadal variability, of monthly maximum daily precipitation over Canada. Also, NAO is correlated with the western monthly maximum daily precipitation at inter-decadal scale. Schulte et al. (2016) Studied the variability of streamflow, precipitation, and temperature in the Mid-Atlantic region of the US and linked to dominant modes of climate variability at annual to multi-decadal timescales. They proved that the influence of climate modes on precipitation,temperature, and streamflow vary from month to month and from season to season.

In Asia, Rathinasamy et al. (2017) studied the standalone teleconnection between precipitation across India and the four climate signals, namely, East Central Tropical Pacific SST(5°N-5°S, 170°-120°W) (Niño 3.4), Pacific Decadal Oscillation (PDO), Southern Oscillation Index (SOI), and Indian Ocean Dipole (IOD) using partial wavelet analysis. They found that the precipitation is only affected by Niño 3.4 and IOD and a non-stationary relationship exists between precipitation and these two climate signals. Using the partial wavelet analysis they showed that SOI and PDO do not significantly affect precipitation. Rathinasamy et al. (2019) used the WCA to detect significant inter-annual and inter-decadal oscillations in monthly precipitation extremes across India and their teleconnections to three prominent climate signals, namely, Niño 3.4, PDO, and IOD. They proved that Niño 3.4 and IOD are the significant drivers of Indian precipitation at inter-annual and inter-decadal scales. They also showed that the strength of influence of large-scale atmospheric circulation patterns on Indian precipitation extremes varies with spatial physiography of the region. Aamir and Hassan (2020) studied the impact of climate signals on precipitation variability in Baluchistan, the biggest province of Pakistan. For this purpose, they used Mann-Kendall statistical test to identify the monthly significant precipitation trends in thirteen meteorological stations located in four regions of Baluchistan. They found that the NAO, Equatorial Indian Ocean Zonal Wind Index (EQWIN), ENSO Modoki Index (EMI) on annual scale, PDO, Atlantic Multi-decadal Oscillation (AMO) on decadal scale are influencing the January precipitation. They also found that ENSO Index (ENSO-MEI), EMI, NAO, PDO and AMO are influencing the June precipitation. Khadgarai et al. (2021) investigated the connection between extreme precipitation variability (intensity, duration, and frequency) over Asian Monsoon and large-scale circulation patterns. They showed that the prevailing conditions of the SST over the equatorial Pacific Ocean are strongly correlated with the variability of extreme precipitation climate change signals through relative phases of SOI, MEI v2, and Niño 3.4 signals.

Recent studies have shown WCA to be a trustworthy method to identify the relationship between precipitation and large-scale climate indicators. Also,

there had been some studies relating precipitation variability to large-scale climate anomalies for Iran. Ghamghami and Bazrafshan (2021) investigated the relationships between sixteen large-scale climate signals with weather types and winter precipitation amounts and patterns over Iran. They employed daily precipitation data during the period 1991–2010 from 130 weather stations across the country. They used several Non-homogeneous Hidden Markov Models (NHMMs) to determine the prevailing weather types governing the spatial distributions of daily precipitation in winter over Iran. They showed that the amounts of winter precipitation at many stations in Iran were significantly correlated with four climate signals, including the AMO, East Atlantic/West Russia (EA/WR) pattern, SOI, and Trans Polar Index (TPI). Dehghani et al. (2020) studied the impact of ENSO, PDO, and NAO on seasonal precipitation over Iran. They used Spearman correlation coefficient between the signals in the previous 12 months with seasonal precipitation, and the meaningful correlations were extracted for 103 synoptic stations with at least 30 years of data. Their results indicated that the SOI, NAO, and PDO have the most impact on seasonal precipitation, respectively. Araghi et al. (2017) studied the linkages between three major climatic signals, AO, NAO and SOI, and precipitation in Iran from 1960 to 2014, at 30 synoptic stations in a time-frequency space, using wavelet coherence. They showed that the SOI is the most effective climatic teleconnection on precipitation in Iran, although the other studied climatic signals have noticeable effects as well. Araghi et al. (2017) applied WCA method for each station separately and studied only three large-scale indicators.

Iran is a vast country, the north of which is influenced by sub-polar large scale atmospheric signals such as North Atlantic Oscillation (NAO), North Sea Caspian Pattern (NCP) and Arctic Oscillation (AO), and the south of the country is impacted by tropical regions and the Indian Ocean atmospheric-ocean signals, including El-Nino Southern Oscillation (ENSO), Indian Ocean Dipole (IOD), Madden Julian Oscillation (MJO). Therefore, large-scale climate signals can have a significant impact on Iran's precipitation variability. On the other hand, there are the following deficiencies in the studies conducted in this field: [1] a limited number of large-scale climate signals have been considered. [2] The effect of signals on all-country precipitation has not been investigated, and previous studies have only examined the impact of signals on stations precipitation. [3] The correlation and regression methods have been used in most previous studies and the WCA as a powerful tool in testing possible linkages between two signals, which are highly irregular, complex, and intermittent non stationary, rarely has used. Due the importance of the subject, our main objective is a more comprehensive study to cover the above deficiencies. Therefore, we considered twenty large-scale climate signals for which data were available. Also, for the precipitation variable, Iran's monthly precipitation is calculated using the Thiessen method for period 1960-2018. The WCA method is applied for investigating the relationship between twenty large-scale signals and the monthly precipitation.

The paper is organized as follows. Section 2 introduces the study area details of used datasets. The proposed approach and methods of analysis are presented in Section 3. Some discussions about the results are provided in Section 4 and finally, Section 5 contains the conclusions.

2 Study Area and Data

2.1 Study Area

Iran covers $1,648,195$ km^2 between 44°E and 63°25′E longitude and 25°N and 38°39′N latitude in south west Asia. It is bordered to the north by the Caspian Sea and to the south by the Persian Gulf and the Gulf of Oman. The Zagros Mountains are the main mountain chain in Iran, which extends form the north-west to the south-east. The other mountain range is the Alborz Mountains, narrow and high mountains that rim the Caspian Sea littoral in the North. The centre of Iran is covered by several closed basins called the Central Plateau. The precipitation variability over Central Plateau of Iran is higher than other regions due to their arid and warm climate (Babaeian and Rezazadeh (2018)).

2.2 Precipitation

The daily precipitation data at 37 station were collected from the Iran Meteorological Organization (IRIMO) for the period 1960 to 2018 (Figure 1). Quality control of data including filling the missing data, deleting outliers due to error, and data homogenization was performed (see Javanshiri et al. (2021) for the procedures). For each station, the monthly precipitation was calculated. Then, the average monthly precipitation of Iran was determined using Thiessen method (Thiessen (1911)). The linear trends and seasonality were extracted from monthly series and after standardization they were used for wavelet analysis.

Figure 2 (left plot) shows the frequency of the total annual precipitation during the 59-year period of 1960-2018. The distribution of annual precipitation is almost normal, meaning that the annual precipitation between 250 to 300 mm constitutes the highest frequency, while annual precipitation more than 400 mm or less than 200 mm is rare. The time series of annual precipitation in Figure 2 (right plot) shows cyclic movements with a upward trend before 1980 and a downward trend at the latter stage. The least amount of total precipitation recorded was 164.4 mm (measured in 2010) while the highest total rainfall was 404.5 mm (measured in 1982).

2.3 Large-Scale Climate Signals

A brief description of the twenty climate signals employed in this study is presented in Table 1. The monthly time series of climate signals were obtained from the Climate Prediction Center and National Climatic Data Center, National Oceanic and Atmospheric Administration (http://www.cpc.ncep.noaa.gov, https://www.ncdc.noaa.gov) for the period

Fig. 1: Map of Iran showing geographic locations of 37 stations considered in the present study.

1960–2018. The linear trends and seasonality were extracted from the series and after standardization they were used for WCA.

Table 1: Summary of climate signals used in this study

Index	Description
WPI	**Western Pacific Index.** The WP pattern is a primary mode of low-frequency variability over the North Pacific in all months, and has been previously described by both Barnston and Livezey (1987) and Wallace and Gutzler (1981).

Table 1: continued from previous page

EA/WR	**Eastern Asia/Western Russia.** The East Atlantic/ West Russia pattern is one of three prominent teleconnection patterns that affects Eurasia throughout year. This pattern has been referred to as the Eurasia-2 pattern by Barnston and Livezey (1987). The East Atlantic/ West Russia pattern consists of four main anomaly centres. The positive phase is associated with positive height anomalies located over Europe and northern China, and negative height anomalies located over the central North Atlantic and north of the Caspian Sea.
NAO	**North Atlantic Oscillation.** The NAO combines parts of the East-Atlantic and West Atlantic patterns originally identified by Wallace and Gutzler (1981) for the winter season. The NAO consists of a north-south dipole of anomalies, with one center located over Greenland and the other center of opposite sign spanning the central latitudes of the North Atlantic between 35°N and 40°N.
NP	**North Pacific pattern.** The NP is the area-weighted sea level pressure over the region 30°N-65°N, 160°E-140°W (Trenberth and Hurrell (1994)).
SOI	**Southern Oscillation Index.** The SOI measures the difference in observed sea level pressure between Tahiti at 18°S, 150°W, and Darwin, Australia, at 12°S, 130°E.
AO	**Arctic Oscillation.** The AO is the Northern Hemisphere annular mode and characterized by winds circulating around the Arctic at a latitude of around 55°N Araghi et al. (2017).
QBO	**Quasi-Biennial Oscillation.** The QBO is a quasi-periodic oscillation of the equatorial zonal wind between easterlies and westerlies in the tropical stratosphere with a mean period of 28 to 29 months.
Niño 1.2	**Extreme Eastern Tropical Pacific SST.** The Niño 1.2 is the average SST anomaly in the region bounded by 0° to 10° S, from 90° to 80°W.
Niño 4	**Central Tropical Pacific SST.** The Niño 4 is the average SST anomaly in the region bounded by 5° S to 5° N, from 160° E to 150°W.
Niño 3.4	**East Central Tropical Pacific SST.** The Niño 3.4 is the average SST anomaly in the region bounded by 5° S to 5° N, from 170° to 120°W.
Niño 3	**Eastern Tropical Pacific SST.** The Niño 3 is the average SST anomaly in the region bounded by 5° S to 5° N, from 150° to 90°W.
BEST	**Bivariate ENSO Timeseries.** The BEST Calculated from combining a standardized SOI and a standardized Niño3.4 SST timeseries.

Table 1: continued from previous page

ONI	**Oceanic Niño Index.** The ONI, a measure of the deviation from normal sea surface temperature in the east-central Pacific Ocean, is the standard index that determines, measures and predicts each El Niño episode.
TNI	**Trans-Niño Index.** The TNI is the difference in normalized SST anomalies between Niño 1.2 and Niño 4 regions. Thus, the TNI measures the gradient in SST anomalies between the central and eastern equatorial Pacific.
TNA	**Tropical Northern Atlantic Index.** The TNA is an indicator of the surface temperatures in the eastern tropical North Atlantic Ocean. It is the SSTs in the box 55° W - 15° W, 5° N - 25° N.
TSA	**Tropical Southern Atlantic Index.** The TSA is an indicator of the surface temperatures in the Gulf of Guinea, the eastern tropical South Atlantic Ocean. It is calculated with SSTs in the box 30°W - 10°E, 20°S - 0°.
WHWP	**Western Hemisphere Warm Pool.** The WHWP is a region of SST warmer than 28.5 °C that extends from the eastern North Pacific to the Gulf of Mexico and the Caribbean, and at its peak, overlaps with the tropical North Atlantic (Wang and Enfield (2001)).
AMM	**Atlantic Meridional Mode.** The AMM is defined as the leading mode of non-ENSO coupled ocean/atmosphere variability in the Atlantic basin. The AMM spatial pattern is defined by applying Maximum Covariance Analysis (MCA) to tropical Atlantic SST and the zonal and meridional components of the 10m wind field over the time period 1950-2005, from the NCEP/NCAR Reanalysis.
NTA	**North Tropical Atlantic Index.** The NAT is an indicator of the surface temperatures in a broad swath of the tropical North Atlantic Ocean. It is calculated with SSTs in the box 40°W - 20°W, 5°N - 20°N.
CAR	**Caribbean Index.** The CAR is the average SST anomalies over the the Caribbean. Data is obtained from the NOAA ERSST V3b dataset. Anomalies were calculated relative to the 1981-2010 climatology, smoothed by three months running mean procedure and projected onto 20 leading EOFs.

3 Methodology

In this section the analysis methods including wavelet transform, wavelet coherence and phase difference will be discussed in details.

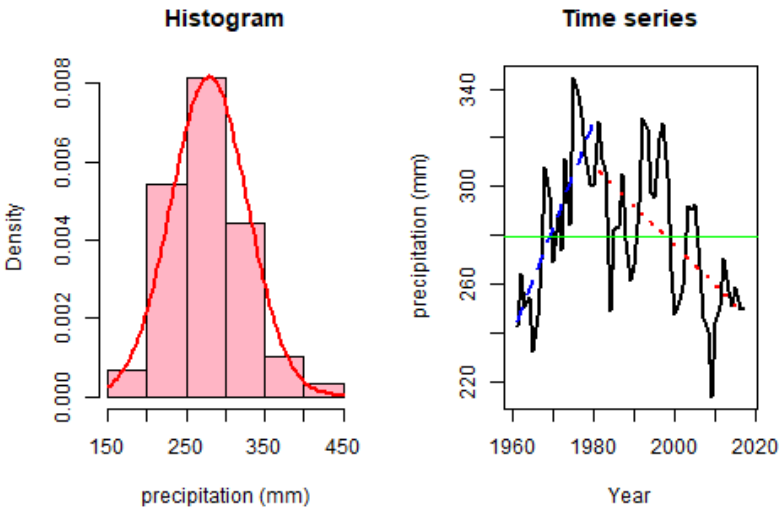

Fig. 2: Histogram and time series of the annual precipitation in Iran for the period 1960-2018

.

3.1 Wavelet Coherence

Cross-wavelet analysis is a tool to measure the relationship between two time series in a time-frequency space. The cross wavelet transform of the two time series x_t and y_t is obtained from the relation with the WT of W_x and W_y as follows (Veleda et al. (2012)):

$$W_{xy}(\tau, s) = \frac{1}{s} . W_x(\tau, s) . W_y^*(\tau, s). \quad (1)$$

Cross wavelet power is the modulus of cross wavelet transform and is obtained from the following equation Grinsted et al. (2004)

$$Power_{xy}(\tau, s) = |W_{xy}(\tau, s)|. \quad (2)$$

The cross wavelet transform can lead to misleading results because it is not normalized. The Wavelet Coherence (WC) solves this problem by normalizing

to the single wavelet power spectrum. The WC between two time series x_t and y_t is given by (Liu et al. (1995))

$$WC = \frac{|S.W_{xy}(\tau, s)|^2}{S.Power_x \times S.Power_y}, \tag{3}$$

where $S.$ is smoothing operator.

3.2 Phase Difference

Relocations of periodic phenomena relative to the localizing origin τ, moved over the time domain, are given by the instantaneous or local wavelet phase which is an angle in the interval $[-\pi, \pi]$ Torrence and Compo (1997)

$$Phase(\tau, s) = Arg(W(\tau, s)) = tan^{-1}\left(\frac{Im(W(\tau, s))}{Re(W(\tau, s))}\right), \tag{4}$$

wherein, $Im(.)$ and $Re(.)$ indicate the imaginary and real part of a given number, respectively. The difference between the x_t and y_t time series phases is called the wavelet phase difference and is calculated as (Torrence and Webster (1999))

$$Angle(\tau, s) = Arg(W_{xy}(\tau, s)) = Phase_x(\tau, s) - Phase_y(\tau, s). \tag{5}$$

If the absolute value is less (more) than $\pi/2$, it indicates that the two series are in-phase (anti-phase). The sign of the phase difference indicates which series is leading. When two series move in-phase, if the phase difference sign is positive (negative), x is leading (lagging). In the case of anti-phase, the positive (negative) sign shows that y is leading (lagging).

4 Results and discussion

The WCA method has been used to investigate the relationship between large-scale signals and precipitation. The WC of precipitation and each of the indicators are computed and corresponding images are plotted using WaveletComp 1.1. packge (Schmidbauer and Roesch (2018)) in R. In the images, there are three components including scale, time and WC. The scale is displayed on the vertical axis and the time on the horizontal axis. Coherence intensity is also shown vertically with the coloured column next to the image. The red parts are surrounded by a white line shows the coherence that was statistically significant at the 95 % confidence level. The cone shape part of the image that is fainter indicates the cone of influence. The values outside the cone of influence should be interpreted and justified with caution.

Phase differences are also shown with directional arrows, where an up and right pointing arrow indicates that the two signals are in-phase and precipitation is leading one, while down and right pointing arrow shows an in-phase

relationship when large climate signal is leading. The left direction of the arrows indicates that the two signals are out of phase, the up (down) pointing arrow shows that the large scale indicator is leading (lagging).

4.1 Atmospheric Signals

Figure 3 shows the WC spectra for precipitation with WP, EA/WR, NAO, NP, SOI, AO and QBO. The WP was found to be coherent with precipitation at 4-8 and 8-16 years scales with an opposite phase difference in early and later part of the record (1960-1974, 1996-2010). The strongest coherence occurs at 4-8 years scale during 1960-1974 (Figure 4a) with the phase difference of 2 years and at 8-16 years scales between 1996-2010 (Figure 4c) with the stable phase difference of 4 years. Also, signals with 16-32 years period (24 years as average) show high in-phase coherence during pre-2000 with a phase difference of 3 years (Figure 4e). Figure 3b demonstrates that there is no significant relationship between EA-WR and precipitation before 1985, and significant relationships have been established in 2-4, 4-8 and 16 years time scales since 1985. It means that controlling role of EW-WR in precipitation of Iran is increasing. The NP has a significant contribution to the precipitation variability at both inter-annual and decadal scales (Figure 3d). There is an out of phase relationship between NP and precipitation at 4-8 years scale during pre-1975 with 2 years of phase difference and 1987-2003 with unstable phase difference (Figure 4b). For the 8-16 years band, the phase change from anti-phase in the 1968s to in-phase in the 1975s and then back to anti-phase in the 1995s (Figure 4d). However, for decadal scale (16-32 years), an anti-phase relationship with 8 years phase difference, where precipitation is leading one, were detected for the pre-1990 period (Figure 4f). Figure 3c shows there is a weak coherence between precipitation and NAO. However, the controlling role of NAO in precipitation at 6-12 months time scale have been increased in recent years. The WC between SOI and precipitation in the bands of 2-4, 4-8 and 8-16 years are statistically significant (Figure 3e). There is an intermittent coherence at 2–4 years, but stable coherence at 4-8 and 8-16 years scales. The analysis of the Figures 4g and 4i reveals that an anti-phase relationship with 3 years phase difference at 4-8 years band during 1985-2003 and an anti-phase relationship with 5 years different phase between precipitation and SOI at 8-16 years scale in the recent decades (1996-2009). It indicates the important control role of this atmospheric pattern on decadal variability of precipitation.

For AO, the coherence with the precipitation is significant at 4-8 years and 8-16 years bands (Figure 3f). The strongest coherence occurs at the inter-decadal scale centred near 16 years (Figure 4j) with in-phase relationship, with AO leading by 2.5 years, during 1973-2005. Comparing to the other signals, there is a strong and long-lasting coherence between Iran's precipitation and AO in inter-decadal scale. Figure 3g shows significant but intermittent coherence between QBO and precipitation at 2–4 and 4–8 years. Also, there is coherence at inra-annual scale (6-12 months) during 1997-2007.

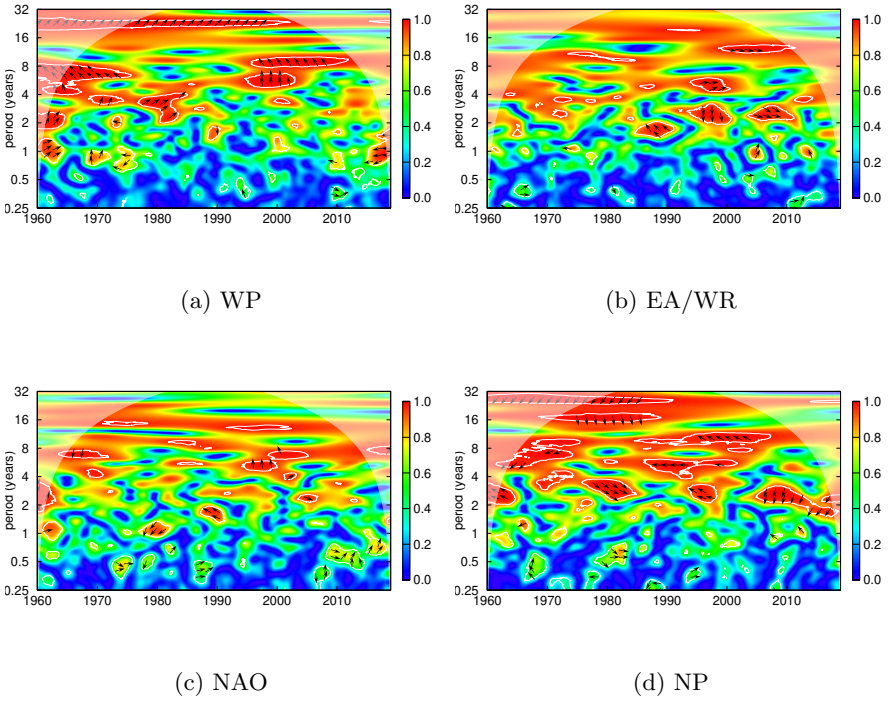

(a) WP

(b) EA/WR

(c) NAO

(d) NP

Fig. 3: Wavelet coherence and phase difference between monthly precipitation and monthly (a)WP, (b) EA (WR), (c) NAO and (d) NP. Vertical coloured column next to the image shows coherence intensity. Shaded areas enclosed by white contours represent WC that is statistically significant at a 5% significance level with respect to a red noise, and the fainter part indicate the cone of influence (COI).

4.2 ENSO-based Signals

Figure 5 shows the WC spectra for precipitation and seven ENSO-based signals. A similar patterns are observed for the coherency between the precipitation and ENSO-based signals included Niño 1.2, Niño 3, Niño 3.4, Niño 4, BEST, ONI and TNI. Most of the high coherence between precipitation and ENSO signals are found at the 2-4 years scale in early and later part of the record and at the 4-8 years scale in the middle of the record for a long period. The longest durations for the 5% significance level regions are detected in the WCs for the Niño 1.2 and Niño 3 at 4-8 years scale. The Figure 6a reveals that their relationship with precipitation are out of phase before 1970 and then it turns to in-phase with phase difference between 0 to 1.5 months. An important point can also be deduced from Figure 5 that a new coherence of of

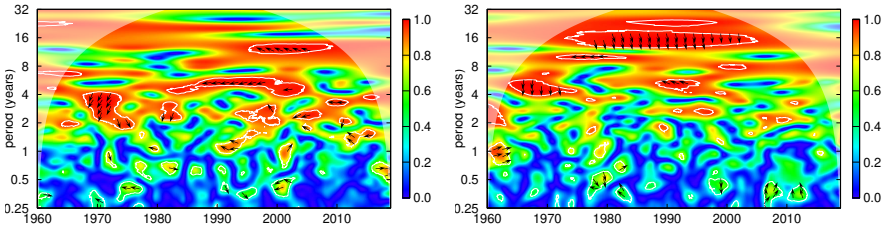

(e) SOI (f) AO

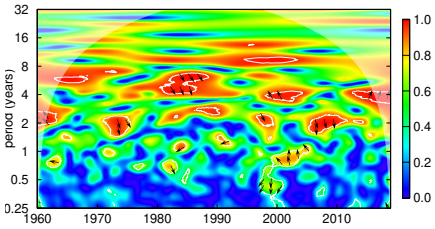

(g) QBO

Fig. 3: Wavelet coherence and phase difference between monthly precipitation and monthly (e) SOI, (f) AO, (g) QBO.

8-16 years has emerged in recent decades between the Iran's precipitation and ENSO-based signals, showing the change of ENSO behaviour from an annual signal to a decadal signal. Figure 5 also shows that a new coherence at 8-16 years scale has emerged in recent decades that shows the ENSO behaviour was changed from annual to decadal signal.

4.3 SST

The WC between precipitation and Atlantic and Pacific SST signals included TNA, TSA, WHWP, AMM, NTA and CAR are shown in Figure 7. The analysis of the Figures 7a and 8d reveals that the most effective period for TNA on precipitation is 2-4 years scale during 1968-1980 with unstable phase difference and during 1988-2002 with phase difference of 2 months. In the last decade, relatively significant coherence have emerged at seasonal to annual periods, while coherency at inter-annual scale have been weakened. It was found that TSA has an anti-phase coherence with precipitation at 4-8 years scale during 1980-1992 and 2000-2003 with approximately 2 years of phase difference. It

should be noted that in the last decade, a coherence between precipitation and TSA has emerged on an 8-16 year scale. The WHWP has a significant contribution to the precipitation variability at 4-8 year scale during 1963-2002. They are in-phase with precipitation leading by 10 months. (Figure 8f). For AMM, the strongest coherence with the precipitation occurs at the decadal scale centred near 24 years during 1965-1995 with AMM leading by 6 years (Figure 7d), but it has been vanished in recent decade. There is also unsteady significant relationship between precipitation and AMM at 1-2 and 2-4 years scales. Figure 8h shows that there is a relationship between NTA and precipitation at 2-4 years scale from 1969 to 1980 with unstable phase difference and during 1988-2002 with 2 months of phase difference. Also, significant coherence have emerged at intra annual scales in the recent years. Although the relationship between CAR and precipitation variability is weak, an annual scale coherence has emerged in recent years.

5 Conclusions

Using WCA, this study investigated the spatio-temporal variability of Iran precipitation with twenty large-scale climate signals. Our findings are summarized as follows:

1. Inter-annual (2–8 years) oscillations were more significant than decadal and inter-decadal oscillations (8–16 years and 16-32 years).
2. At inter-annual scale, Niño 1.2, ONI and WHWP exerted relatively strong influence on Iran precipitation, respectively.
   - precipitation and Niño 1.2 are in-phase with precipitation leading by 1.5 months.
   - precipitation and ONI are out of phase before 1970 with ONI leading by 2.5 years, then they are in-phase till 2006 with precipitation is leading around 1 year and they are again in-phase with ONI is leading 1 year in the ned of the records.
   - precipitation and WHWP are again in-phase; precipitation is leading by less than 10 months.
3. On a decadal and inter-decadal scale, AMM, WP and AO are the most effective climatic indicators on the variability of precipitation in Iran, respectively.
   - precipitation and AMM are out of phase with AMM leading by 6.5 years.
   - precipitation and AO are in-phase; AO leading by 2.5 years.
   - precipitation and WP are again in-phase; precipitation is leading by 3 years.
4. It is suggested to use AMM index for decadal precipitation forecasts and Niño 1.2 and WHWP for seasonal forecasts.

5. Generally, an interesting behaviour change was observed in the coherence between precipitation and large-scale oceanic signals. The coherency in the decadal to inter-decadal scale has been decreased clearly and an instead unsteady coherency in annual scale has been emerging in the recent decade. This confirms that the general behaviour of oceanic signals tend from low frequency signals toward high frequency signals, which decreases the decadal predictability of the climate.

Acknowledgments. The authors would like to thank the anonymous reviewers who reviewed the manuscript constructively and Editors for their comments. The authors declare that there is no conflict of interest.

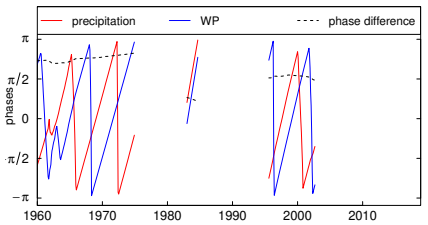

(a) WP, 4-8 years

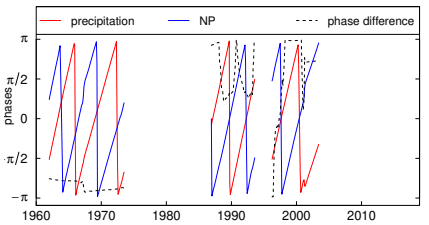

(b) NP, 4-8 years

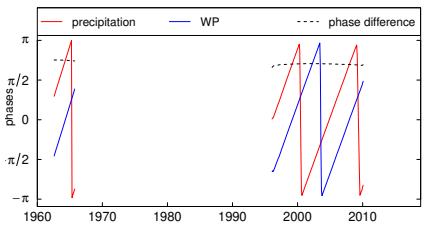

(c) WP, 8-16 years

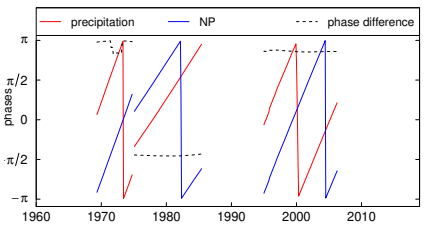

(d) NP, 8-16 years

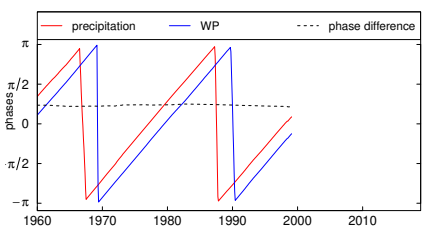

(e) WP, 16-32 years

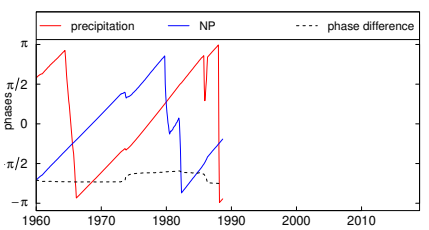

(f) NP, 16-32 years

Fig. 4: Phases differences between monthly precipitation and monthly WP, NP with period 4-8, 8-16 and 16-32 years.

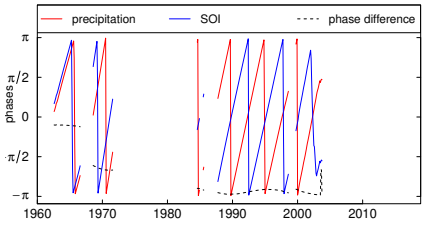

(g) SOI, 4-8 years

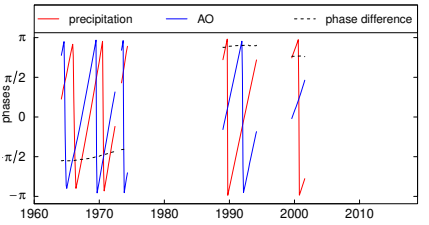

(h) AO, 4-8 years

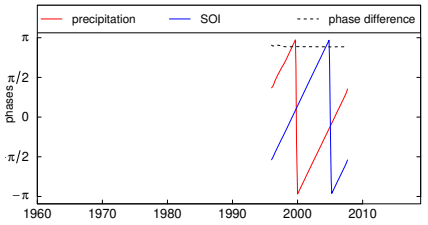

(i) SOI, 8-16 years

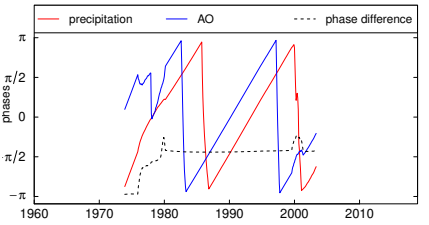

(j) AO, 8 -16 years

Fig. 4: Phases differences between monthly precipitation and monthly SOI, AO with period 4-8, 8-16 years.

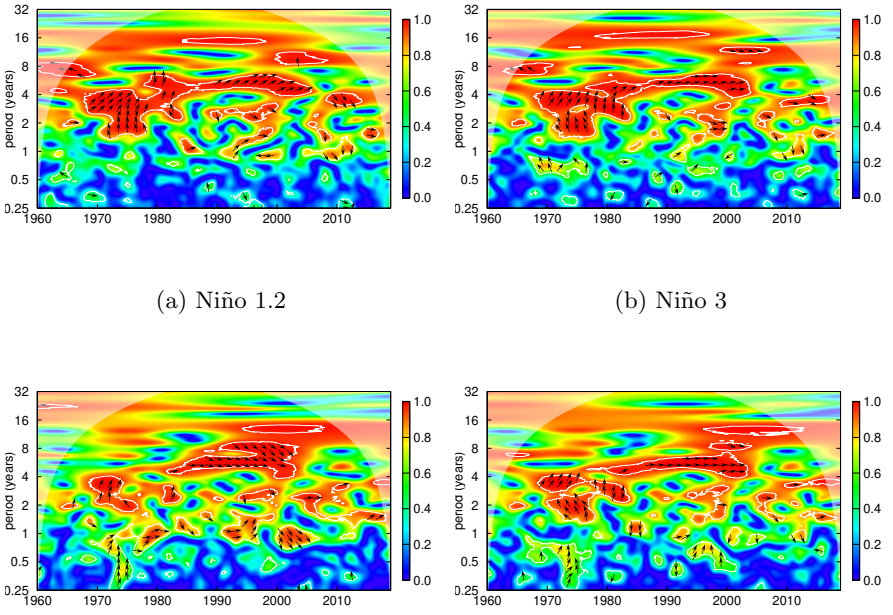

(a) Niño 1.2

(b) Niño 3

(c) Niño 4

(d) Niño 3.4

Fig. 5: Wavelet coherence and phase difference between monthly precipitation and monthly (a) Niño1.2, (b) Niño3, (c) Niño4, (d) Niño3.4.

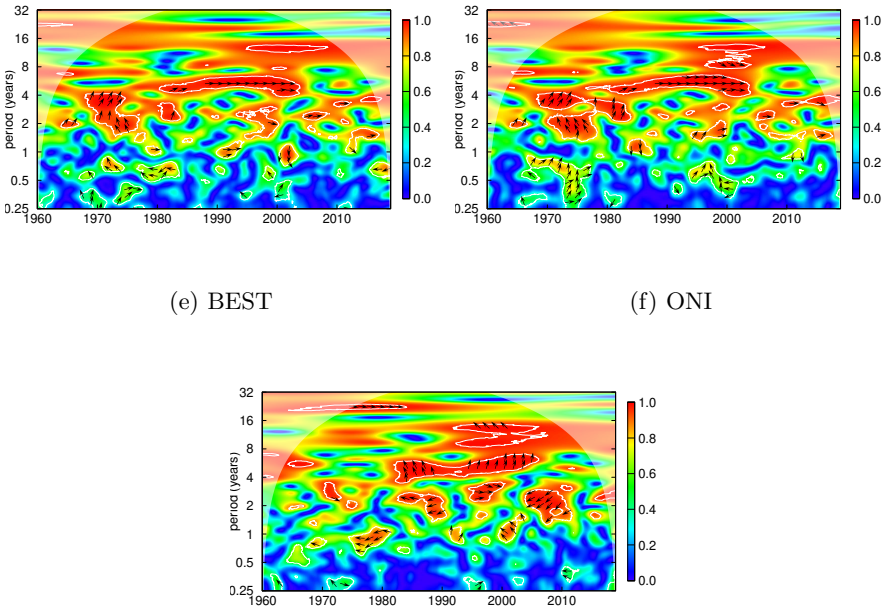

(e) BEST (f) ONI

(g) TNI

Fig. 5: Wavelet coherence and phase difference between monthly precipitation and monthly (e) BSET, (f) ONI, (g) TNI.

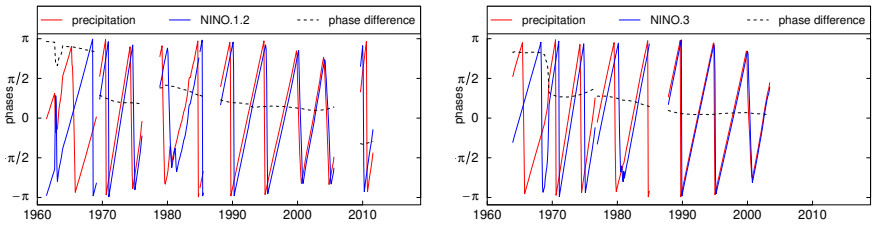

(a) Niño 1.2 , 4-8 years (b) Niño 3, , 4-8 years

Fig. 6: Phases differences between monthly precipitation and monthly Niño 1.2, Niño 3 with period 4-8 years.

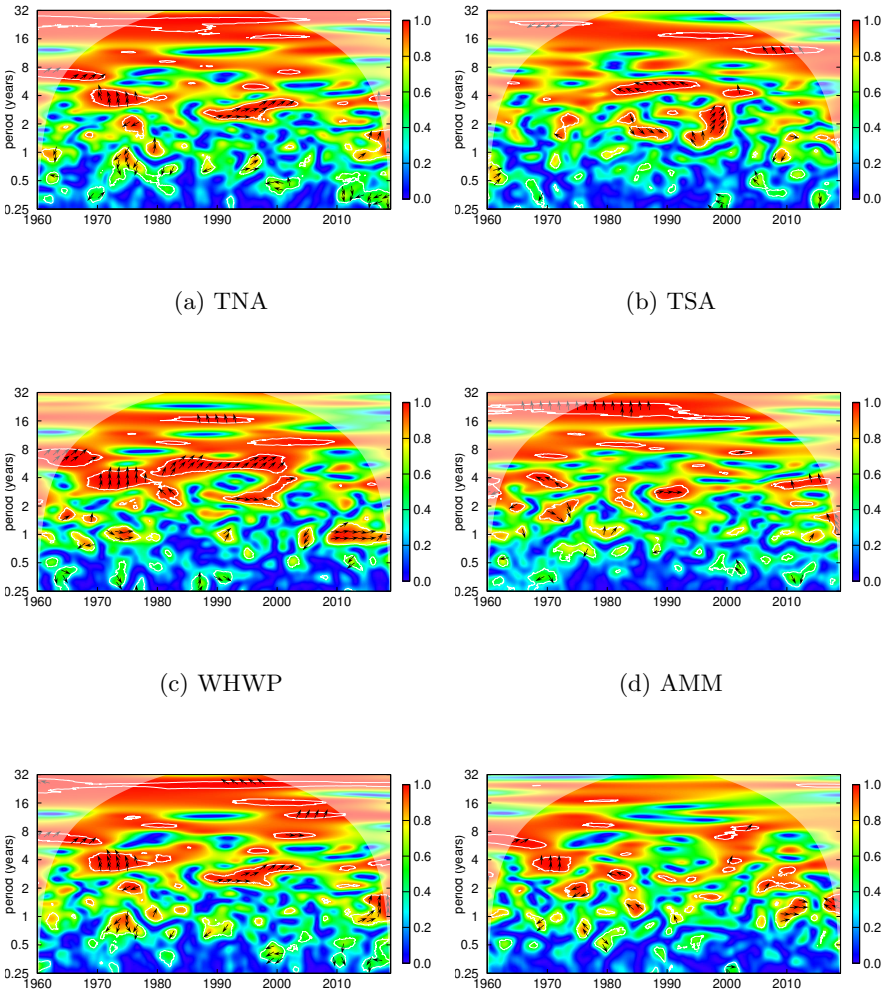

(a) TNA (b) TSA

(c) WHWP (d) AMM

(e) NTA (f) CAR

Fig. 7: Wavelet coherence and phase difference between monthly precipitation and SSTs.

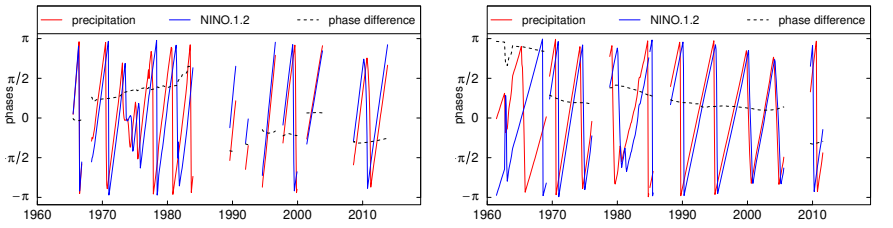

(a) ONI, 2-4 years

(b) ONI, 4-8 years

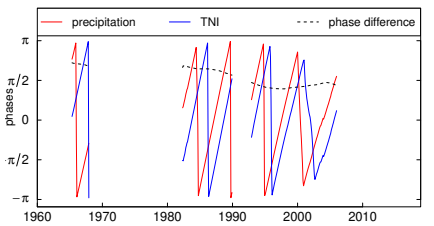

(c) TNI, 4-8 years

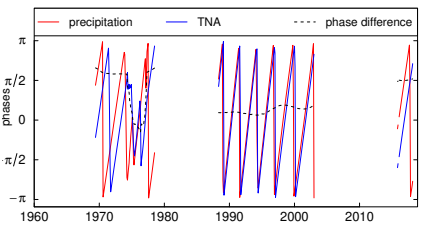

(d) TNA, 2 -4 years

Fig. 8: Phases differences between monthly precipitation and monthly ONI, TNA, TNI with period 2-4 and 4-8 years.

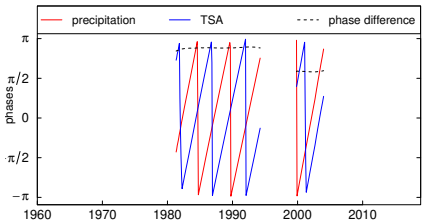

(e) TSA, 4 -8 years

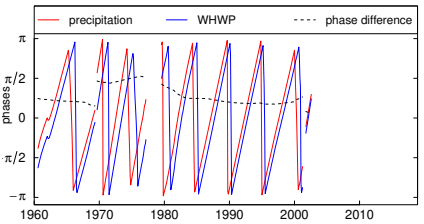

(f) WHWP, 4 -8 years

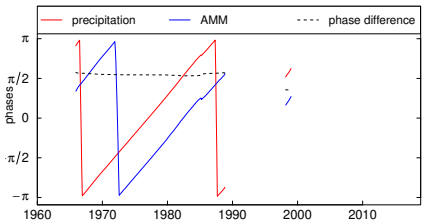

(g) AMM, 16 -32 years

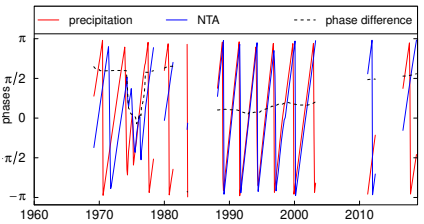

(h) NTA, 2 -4 years

Fig. 8: Phases differences between monthly precipitation and monthly TSA, WHWP, AMM, NTA.

References

Aamir, E. and I. Hassan. 2020. The impact of climate indices on precipitation variability in baluchistan, pakistan. *Tellus A: Dynamic Meteorology and Oceanography 72*(1): 1–46 .

Araghi, A., M. Mousavi-Baygi, J. Adamowski, and C. Martinez. 2017. Association between three prominent climatic teleconnections and precipitation in iran using wavelet coherence. *International Journal of Climatology 37*(6): 2809–2830 .

Babaeian, I. and P. Rezazadeh. 2018, 10. On the relationship between indian monsoon withdrawal and iran's fall precipitation onset. *Theoretical and Applied Climatology* 134. https://doi.org/10.1007/s00704-017-2260-0 .

Barnston, A. and R. Livezey. 1987, 07. Classification, seasonality and persistence of low-frequency atmospheric circulation patterns. *Monthly Weather Review* 115. https://doi.org/10.1175/1520-0493(1987)115⟨1083:CSAPOL⟩2.0.CO;2 .

Chang, N.B., S. Imen, K. Bai, and Y.J. Yang. 2017. The impact of global unknown teleconnection patterns on terrestrial precipitation across north and central america. *Atmospheric Research* 193: 107–124 .

Dehghani, M., S. Salehi, A. Mosavi, N. Nabipour, S. Shamshirband, and P. Ghamisi. 2020. Spatial analysis of seasonal precipitation over iran: Co-variation with climate indices. *ISPRS International Journal of Geo-Information 9*(2): 73 .

Ghamghami, M. and J. Bazrafshan. 2021. Relationships between large-scale climate signals and winter precipitation amounts and patterns over iran. *Journal of Hydrologic Engineering 26*(3): 05021001 .

Grinsted, A., J.C. Moore, and S. Jevrejeva. 2004. Application of the cross wavelet transform and wavelet coherence to geophysical time series. *Nonlinear processes in geophysics 11*(5/6): 561–566 .

Javanshiri, Z., M. Pakdaman, and Y. Falamarzi. 2021. Homogenization and trend detection of temperature in iran for the period 1960–2018. *Meteorology and Atmospheric Physics*: 1–18 .

Jemai, S., M. Ellouze, and H. Abida. 2017. Variability of precipitation in arid climates using the wavelet approach: case study of watershed of gabes in south-east tunisia. *Atmosphere 8*(9): 178 .

Jevrejeva, S., J. Moore, P. Woodworth, and A. Grinsted. 2005. Influence of large-scale atmospheric circulation on european sea level: results based

on the wavelet transform method. *Tellus A: Dynamic Meteorology and Oceanography 57*(2): 183–193 .

Jiang, R., T.Y. Gan, J. Xie, and N. Wang. 2014. Spatiotemporal variability of alberta's seasonal precipitation, their teleconnection with large-scale climate anomalies and sea surface temperature. *International journal of climatology 34*(9): 2899–2917 .

Khadgarai, S., V. Kumar, and P.K. Pradhan. 2021. The connection between extreme precipitation variability over monsoon asia and large-scale circulation patterns. *Atmosphere 12*(11): 1492 .

Liu, P., E. Oufoula-Georgiou, and P. Kumar. 1995, 01. Wavelet spectrum analysis and ocean wind waves. *Wavelets in Geophysics*: 151–166 .

Ouachani, R., Z. Bargaoui, and T. Ouarda. 2013. Power of teleconnection patterns on precipitation and streamflow variability of upper medjerda basin. *International Journal of Climatology 33*(1): 58–76 .

Pakdaman, M., I. Babaeian, Z. Javanshiri, and Y. Falamarzi. 2022. European multi model ensemble (emme): A new approach for monthly forecast of precipitation. *Water Resources Management*: 1–13 .

Pakdaman, M., Y. Falamarzi, I. Babaeian, and Z. Javanshiri. 2020. Post-processing of the north american multi-model ensemble for monthly forecast of precipitation based on neural network models. *Theoretical and Applied Climatology 141*(1): 405–417 .

Pakdaman, M., S.S. Naghab, L. Khazanedari, S. Malbousi, and Y. Falamarzi. 2020. Lightning prediction using an ensemble learning approach for northeast of iran. *Journal of Atmospheric and Solar-Terrestrial Physics* 209: 105417 .

Rathinasamy, M., A. Agarwal, V. Parmar, R. Khosa, and A. Bairwa. 2017. Partial wavelet coherence analysis for understanding the standalone relationship between indian precipitation and teleconnection patterns. *arXiv preprint arXiv:1702.06568* .

Rathinasamy, M., A. Agarwal, B. Sivakumar, N. Marwan, and J. Kurths. 2019. Wavelet analysis of precipitation extremes over india and teleconnections to climate indices. *Stochastic Environmental Research and Risk Assessment 33*(11): 2053–2069 .

Schmidbauer, H. and A. Roesch. 2018, 03. Waveletcomp 1.1: A guided tour through the r package .

Schulte, J.A., R.G. Najjar, and M. Li. 2016. The influence of climate modes on streamflow in the mid-atlantic region of the united states. *Journal of Hydrology: Regional Studies* 5: 80–99 .

Tan, X., T.Y. Gan, and D. Shao. 2016. Wavelet analysis of precipitation extremes over canadian ecoregions and teleconnections to large-scale climate anomalies. *Journal of Geophysical Research: Atmospheres 121*(24): 14–469 .

Thiessen, A. 1911, 01. Precipitation averages for large areas. *Monthly Weather Review - MON WEATHER REV* 39. https://doi.org/10.1175/1520-0493(1911)39⟨1082b:PAFLA⟩2.0.CO;2 .

Torrence, C. and G. Compo. 1997, 10. A practical guide to wavelet analysis. *Bulletin of the American Meteorological Society* 79. https://doi.org/10.1175/1520-0477(1998)079⟨0061:APGTWA⟩2.0.CO;2 .

Torrence, C. and P. Webster. 1999, 08. Interdecadal changes in the enso-monsoon system. *Journal of Climate - J CLIMATE* 12. https://doi.org/10.1175/1520-0442(1999)012⟨2679:ICITEM⟩2.0.CO;2 .

Trenberth, K. and J. Hurrell. 1994, 03. Decadal atmosphere-ocean variations in the pacific. *Climate Dynamics* 9: 303–319. https://doi.org/10.1007/BF00204745 .

Veleda, D., R. Montagne, and M. Araujo. 2012, 09. Cross-wavelet bias corrected by normalizing scales. *Journal of Atmospheric and Oceanic Technology* 29: 1401–1408. https://doi.org/10.1175/JTECH-D-11-00140.1 .

Wallace, J. and D. Gutzler. 1981, 01. Teleconnections in the geopotential height field during the northern hemisphere winter. *Monthly Weather Review* 109: 784–812. https://doi.org/10.1175/1520-0493(1981)109x0003C;0784:titghf⟩2.0.co;2 .

Wang, C. and D. Enfield. 2001, 04. The tropical western hemisphere warm pool. *Geophysical Research Letters* 28: 1635–1638. https://doi.org/10.1029/2000GL011763 .